Molecular reductant-induced control of a graphene-organic interface for electron injection

Fengyu Zhang[†], Chen Klein[‡], Elena Longhi[§], Stephen Barlow[§], Seth R. Marder[§], Gabby Sarusi[‡] and Antoine Kahn[*,†]

[†]Department of Electrical Engineering, Princeton University, Princeton, New Jersey 08544, USA

[‡]Department of Electro-Optics and Photonics Engineering and Ilsa Katz institute for nanoscience and nanotechnology, Ben-Gurion University of the Negev, Be'er Sheva 8410501, Israel

[§]Center for Organic Photonics and Electronics and School of Chemistry and Biochemistry, Georgia Institute of Technology, Atlanta, Georgia 30332-0400, USA

[†,‡]Similar contributions by Fengyu Zhang and Chen Klein to this work

ABSTRACT: Surface doping of graphene with redox-active molecules is an effective approach to tune its electrical properties, in particular for application as transparent electrodes. Here we present a study and application of surface n-doping of graphene with the molecular reductant (pentamethylcyclopentadienyl)(1,3,5-trimethylbenzene)ruthenium dimer ([RuCp*Mes]$_2$). Photoemission spectroscopy and carrier-transport measurements are combined to investigate doping-induced changes in the electronic structure of the interface between graphene and phenyldi(pyren-2-yl)phosphine oxide ($POPy_2$), which is a low-electron-affinity material that has been used as an electron-transport layer (ETL) in organic light-emitting diodes. Photoemission and Hall-voltage measurements confirm the n-doping of graphene. Doping with 1-2 nm of [RuCp*Mes]$_2$ reduces the graphene work function by 1.8 eV and the electron injection barrier by more than 1 eV, enhancing electron injection into $POPy_2$ by several orders of magnitude. Graphene/$POPy_2$/Al diodes with doped graphene cathodes exhibit reasonable stability both in nitrogen and air. These results represent a significant step toward the use of graphene as a transparent cathode for organic devices in general and for OLEDs in particular.

■ INTRODUCTION

The properties of transparent conducting electrodes (TCE) are crucial to the design of state-of-the-art organic light-emitting diodes (OLED). Three main criteria are typically used to evaluate a TCE layer: low sheet resistance, high transmittance, and proper energy alignment between the Fermi level of the electrode and the frontier orbitals of the organic semiconductor with which it forms an interface.[1] To date, indium tin oxide (ITO) has been widely used as a TCE material in OLEDs, due to its exceptional electrical properties[2] and high transparency.[3] However, ITO is expensive and brittle, and thus unsuitable for flexible applications, and is known to release indium ions, which diffuse into the active layers, resulting in device degradation.[4] Moreover, its work function (WF) is generally suitable for use as an anode, but, at least without further modification, not as a cathode. The mechanical properties and transparency of single- to few-layer graphene [5] are attractive for a number of applications, including the TCE of flexible OLEDs.[5,6] However, its WF (~ 4.5 eV)[7], like that of ITO, is relatively high and typically unsuitable for use as a cathode in OLEDs. In general, doping is an effective method to circumvent this issue and manipulate the electrical properties of graphene by tuning its WF, leading to higher device performance.[6,8–14] In addition, the relatively high sheet resistance of single-layer graphene (> 300 Ω/sq)[15], compared to that of ITO (10-20 Ω/sq), could be reduced upon doping.[6,8] n-Doping of graphene has been achieved via alkali metal deposition,[16] substitutional doping,[17,18] alkali metal carbonates,[19,20] transition metals,[21,22] gases,[23–25] and molecular doping.[1,26–28] The first two methods, which are the most common in graphene n-doping, however, present some difficulties. Alkali metals are unstable in air, and their deposition on graphene is known to cause damage, leading to a significant reduction in carrier mobility.[17,19,29] In addition, alkali-metal ions may diffuse into adjacent organic layers. Substitutional doping requires high processing temperatures and, more importantly, involves covalent bonding of the dopant to graphene, which perturbs the hexagonal carbon lattice and induces structural and electronic distortions.[30,31] In contrast, doping by adsorption of reducing organic and metal-organic molecules onto the graphene sheet preserves the structure and is less perturbing than substitutional doping.[18] Such molecules have been shown to be adsorbed onto graphene without forming a covalent bond, and can decrease the sheet resistance with minimal impact on carrier mobility.[1,32]

The molecular reductant 2-(2-methoxyphenyl)-1,3-dimethyl-2,3-dihydro-1*H*-benzoimidazole (o-MeO-DMBI) has been used on graphene and led to an air-stable decrease of the WF by 0.70 eV.[33] However, this decrease is generally

insufficient for electron injection into transport material with an electron affinity (EA) smaller than 3 eV.[34] Recently, organometallic dimers have been found to reduce the WF of various conducting electrodes effectively by either deposition in vacuum or drop-casting from solution.[28,35,36] Mansour et al. reported the largest reduction in WF (1.5 eV) for graphene to date for solution-based doping using (pentamethylcyclopentadienyl)(1,3,5-trimethylbenzene)ruthenium dimer ($[RuCp^*Mes]_2$).[1,37] In this work, we investigate the surface doping of a single graphene sheet by deposition of $[RuCp^*Mes]_2$ (Figure 1b), using contact potential difference (CPD), ultraviolet photoelectron spectroscopy (UPS), and Hall-effect measurements. We show here a nearly 2 eV decrease of the graphene WF (from 4.5-4.8 eV to 2.6 eV), resulting in part from a surface dipole formed by electron transfer from the dopant monomers to the graphene, and, in part, from an upward shift of the Fermi level into the graphene conduction-band states. We build diodes that demonstrate improved electron injection from the doped graphene into the low EA electron-transport material phenyldi(pyren-2-yl)phosphine oxide ($POPy_2$, EA = 2.2 eV) (Figure 1a). This investigation allows a better understanding of the interface between graphene and an organic layer, and of the potential role of graphene as a transparent electron-injection contact in organic devices.

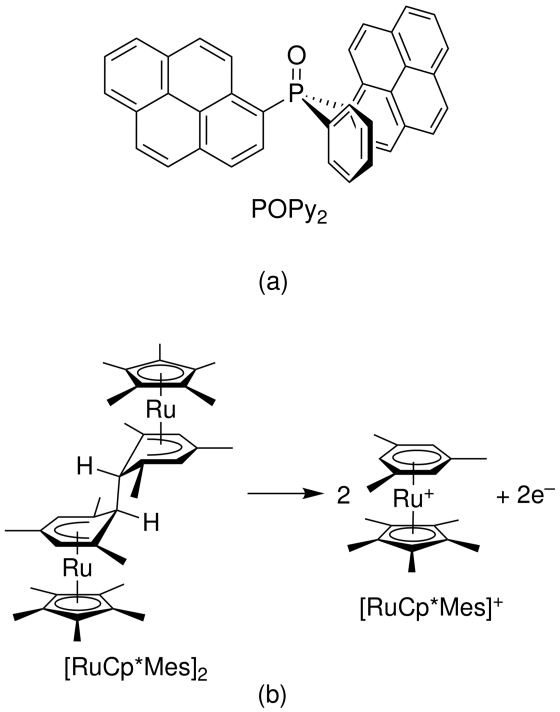

Figure 1. (a) Chemical structure of $POPy_2$ and (b) chemical structure of $[RuCp^*Mes]_2$ and its overall doping reaction to form two $[RuCp^*Mes]^+$ cations and to release two electrons.

■ EXPERIMENTAL SECTION

Preparation of Graphene: Single layer graphene was grown by chemical vapor deposition (CVD) on 18 μm thick copper catalyst foil and cut into 6 × 4 cm^2 samples. These samples were transferred to a Si/SiO_2 (2.5 × 2.5 cm^2 or 1 × 1 cm^2) substrate using a wet transfer process. The transfer of graphene from the copper foil was done using poly(methyl methacrylate) (PMMA), dissolved in chlorobenzene with a concentration of 50 mg ml^{-1}. The PMMA solution was first spin-coated on graphene/copper foil for 50 s at a speed of 4500 rpm. The graphene/copper foil was left in air for one day to allow the drying of the PMMA. Then PMMA-coated graphene was etched with aqueous solution of 0.4 M $FeCl_3$, followed by rinsing in HCl (32%). The graphene was then rinsed in DI water and transferred onto Si/SiO_2 substrate. The PMMA was then removed in acetone for 30 min.

UPS and vacuum Kelvin probe (Vac-KP): The dopant $[RuCp^*Mes]_2$ was synthesized as previously described.[38] $POPy_2$ (purity > 99%) was purchased from Luminescence Technology and used as received. $[RuCp^*Mes]_2$ and $POPy_2$ layers were deposited via thermal evaporation under ultra-high vacuum (UHV, base pressure less than 1 x 10^{-9} Torr). Prior to the deposition of $POPy_2$, the surface doped graphene was activated with 375 nm photons (Thorlabs, M375L3 LED) for 15 s. The n-doped $POPy_2$ films were co-evaporated, with host and dopant evaporation rates controlled by quartz crystal microbalances. The doping molar ratio (mol%) was defined as the percentage of dopant molecules per total number of host molecules, i.e., ($N_{[RuCp^*Mes]2}$/N_{POPy2}) × 100%. The CPD measurements using the Vac-KP were done in an interconnected chamber. The samples were transferred under UHV to the analysis system (p < 5 x 10^{-10} Torr), and measured with UPS using the He I ($h\nu$ = 21.22 eV) photon line of a He discharge lamp. For each UPS spectrum, the emission features due to satellite line excitations of the He discharge lamp were subtracted. The experimental resolution for UPS was 0.15 eV, and the Fermi level reference in UPS was determined with a clean Au substrate.

Hall-effect measurement: For Hall-effect measurements, the surface-doped graphene samples were prepared in a thermal evaporator (Angstrom Engineering, Inc.) connected to a glovebox ($O_2 \leqslant$ 0.1 ppm). Aluminum contacts were fabricated via evaporation through a shallow mask. The doped graphene films were encapsulated in the glovebox with epoxy (LT-U001UV Adhesive, Lumtec) to mitigate the effects of air exposure. Hall effect measurements were performed at room temperature in air, using the van der Pauw method with a reversible sweep of magnetic field up to 3600 G. The changes in the transverse voltage were measured with DC excitation currents of 0 mA, -1 mA, and 1 mA. Details on the encapsulation, calculation of carrier density and calculation of Hall mobility are shown in Supporting Information.

Field-effect transistor (FET) measurement: The CVD-grown single-layer graphene was transferred onto a 300 nm SiO_2 on Si substrate. 100 nm of aluminum was evaporated on top with a shallow mask to contact the graphene as drain and source electrodes. The dimension of the graphene FET channel was about 4 mm x 4 mm. The backside of the Si substrate was scratched with a diamond knife to remove the native oxide, followed by backside-metalization with indium. The FET with doped graphene was UV-activated (375 nm OLEDs, 15 s) and measured in a dark box. All graphene

FETs were fabricated and characterized in the N_2 glovebox with O_2 less 0.1 ppm.

■ RESULTS AND DISCUSSION

Changes induced by evaporation of $[RuCp^*Mes]_2$ onto a graphene surface were first evaluated via UPS. The secondary electron cutoff (SECO) and the top of the valence band are displayed in Figures 2a and 2b, respectively. The graphene WF, determined by linear extrapolation of the SECO, decreases from 4.45 eV to 2.62 eV with the deposition of a nominal 1 nm layer of $[RuCp^*Mes]_2$. The top of the valence band undergoes a radical change. The spectrum of the as-loaded graphene shows the monotonic decrease expected from the graphene density of state close to E_F. In contrast, the spectrum of the doped surface shows a new emission feature extending above E_F, with a dip around -0.55 eV attributed to the Dirac point (DP). The changes in UPS spectra are similar to those observed by Paniagua et al. when doping graphene with the solution-deposited 1,2,3,4,5-pentamethylrhodocene dimer,[28] in both cases indicating a shift of E_F to well above the DP due to the filling of the conduction band states by electrons transferred from the dimeric dopants.

Ultra-violet irradiation, which is necessarily present during UPS measurements, may contribute to the photo-activation of the doping process, as previously shown by Lin et al. in the case of n-doping $POPy_2$.[39] In order to gauge the impact of $[RuCp^*Mes]_2$ on graphene without interference by UV photons, we investigated the graphene WF via CPD using a Vac-KP, before and after irradiation with an independent UV source. As shown in Figure 3a, the UPS and CPD measurements of the as-loaded graphene show different initial WFs, presumably due to the effect of UV on graphene surface contaminants.[40] The Vac-KP CPD measurements show that the WF of as-loaded graphene decreases without photoactivation from 4.75 eV to 3.50 eV following the deposition of 1 nm $[RuCp^*Mes]_2$. This is attributed to electron donation by a fraction of the $[RuCp^*Mes]_2$ dopants to easily reduced conduction states in graphene. Additional doping is achieved with a 15 s UV-activation (375 nm LED), which lowers the WF from 3.50 eV to 2.60 eV, consistent with the value obtained from UPS where the measurement inevitably involves UV irradiation.

This behavior is consistent with the known solution doping mechanism for $[RuCp^*Mes]_2$; the initial step is an exergonic to moderately endergonic electron transfer from the dimer to an acceptor, which is followed by cleavage of the resultant dimer cation, $[RuCp^*Mes]_2^{\bullet+}$, to give the highly reducing [RuCp*Mes] monomer, which then reduces a second acceptor, and a $[RuCp^*Mes]^+$ cation.[41] The solution oxidation potential of the dimer is ca. −1.0 V vs. ferrocene, which corresponds to an approximate ionization energy (IE) of 3.8 eV, suggesting that initial electron transfer to graphene would be exergonic. However, as the extent of graphene doping increases, this electron transfer becomes increasingly endergonic – owing to the upward shift in E_F, the increased interface dipole, and cation-cation repulsions on the surface – and so the rate of thermal electron transfer from dimer to acceptor becomes negligible. However, if further doping is still thermodynamically viable (the effective redox potential of the dimer is ca. −2.0 V, equivalent to an effective IE of ca. 2.8 eV), photoirradiation may help overcome the kinetic barrier. In the present system (where the graphene is weakly absorbing), this might occur through electron transfer from photoexcited $[RuCp^*Mes]_2$ to the graphene to form $[RuCp^*Mes]_2^{\bullet+}$ (with subsequent cleavage and electron transfer), or perhaps from cleavage of photoexcited $[RuCp^*Mes]_2$ (with subsequent electron transfers from the monomers to graphene). Similar photoinduced doping has been seen in various dimer:acceptor systems, including the solution reactions of other dimers with various acceptors[38,42] and the solid-state doping of $POPy_2$ with $[RuCp^*Mes]_2$,[39] although the dominant pathways likely involve dimer-to-photoexcited acceptor electron transfer and/or (in the solid state) photoexcitation of dimer:acceptor charge-transfer complexes. In the case of $[RuCp^*Mes]_2$:$POPy_2$, photodoping enables metastable doping beyond the expected thermodynamic limit, likely due to the barriers associated with rereduction and redimerization of the dopant species.[39]

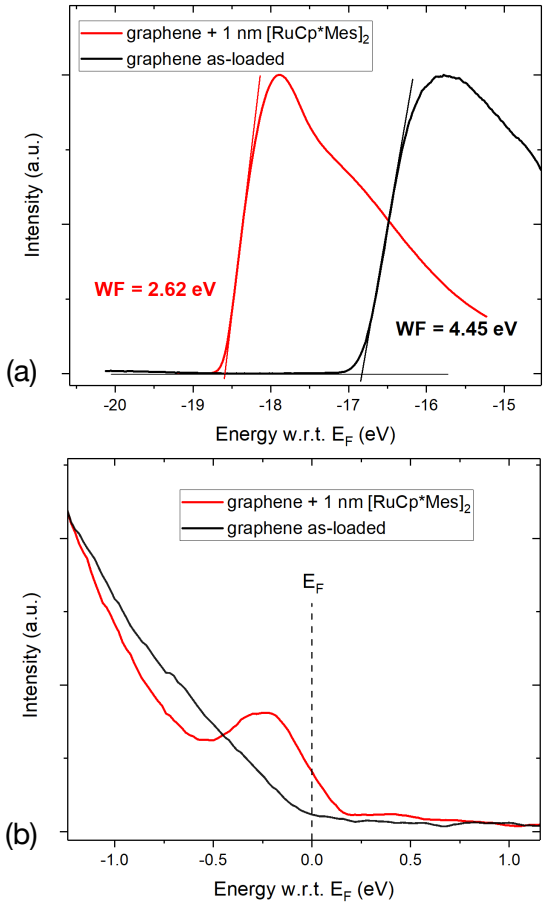

Figure 2. UPS spectra of as-loaded graphene and surface-doped graphene. (a) photoemission cut-off and (b) valence-band region.

When the UV-activated graphene film was kept in the dark under ultra-high vacuum (UHV, 10^{-9} Torr) and re-measured after one week, a 0.4 eV increase in WF was observed. Upon re-activation (15 s, 375 nm LED), the WF recovers its initial photo-activated value (2.6 eV). The mechanism of the reversible 0.4 eV increase in WF during the week in the dark is not known at this point. However,

contaminants may remove the highest-lying electrons from the heavily n-doped graphene, with photoirradiation leading to re-activation and doping by unreacted dimers on the surface. To further investigate the influence of the amount of dopants on the graphene WF, Vac-KP measurements were performed before and after UV-activation upon increasing deposition of $[RuCp^*Mes]_2$ (Figure 3b). The WF of non-activated samples decreases with increasing dopant deposition, but the WF following activation reaches its 2.6 eV minimum with just 1 nm. To ensure a uniform coverage by the dopant layers and a consistent WF after activation, we chose a nominal deposition of 2 nm for the transport and interface measurements.

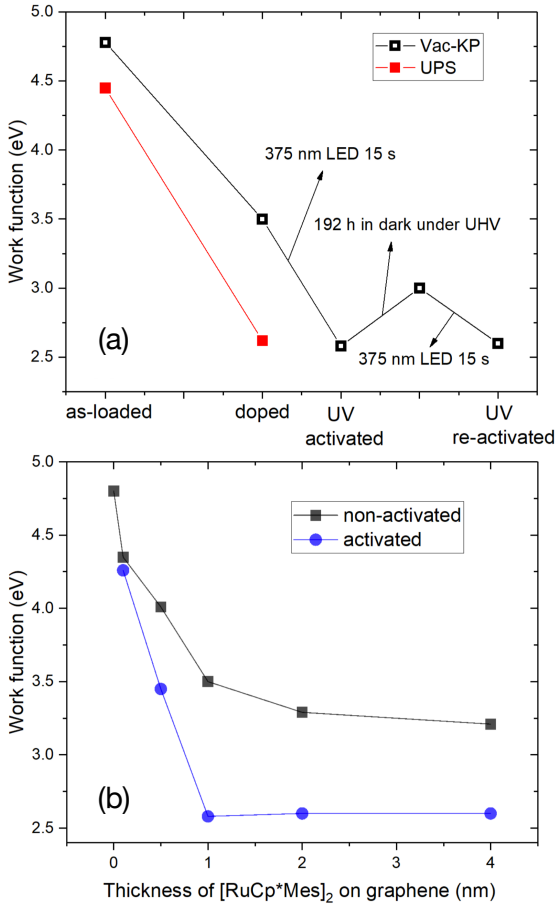

Figure 3. (a) Change in work function of graphene upon doping, determined by UPS and Vac-KP; (b) change in work function measured via Vac-KP, before and after UV-activation, as a function of increasing dopant thickness.

To further test the impact of surface dopants on carrier type and density in the graphene film, graphene field-effect transistors (GFETs) were built and current-voltage characteristics measured, with both as-loaded and surface-doped graphene. Figure 4 shows the drain current I_{DS} measured for a constant drain-source voltage V_{DS} = 100 mV as a function of the gate voltage applied on the backside of the Si/SiO_2 substrate. The GFETs with as-loaded graphene shows a small positive DP voltage at about 12 V, suggesting a p-type character of the material exposed to air. The behavior is mainly due to the poly(methyl methacrylate) (PMMA) residue on the surface of the CVD graphene introduced during transfer.[43] The defects caused by exposure to oxygen and moisture as well as the coupling to the SiO_2 are also generally found to result in p-doping in graphene.[40] As a result, the minimum conductivity corresponding to the DP voltage is shifted to positive voltages instead of being around 0 V, consistent with several previous studies.[1,44] In contrast, the graphene doped with a 2 nm film of dimers and UV-activated shows a clear n-type behavior with the DP voltage shifted to -30 V. The shift in DP voltage is consistent with the transfer of electrons from $[RuCp^*Mes]_2$ dimers to the graphene layer.

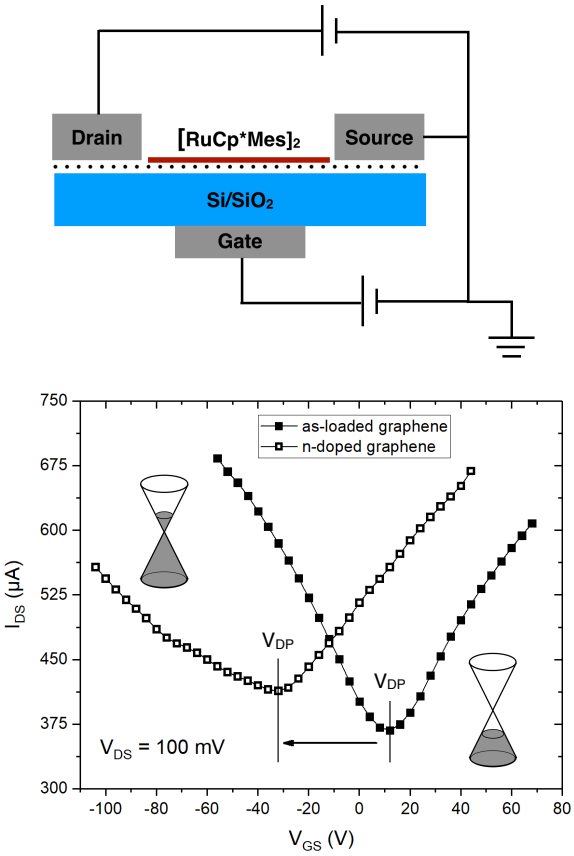

Figure 4. Schematic of back gate GFETs with $[RuCp^*Mes]_2$ dimers doping on the surface (top); transfer curve of as-loaded and n-doped GFETs (bottom).

Room temperature Hall-effect measurements were performed on as-loaded and n-doped graphene using the van der Pauw method. Results are summarized in Table 1. The sheet resistance (Rs) of as-loaded graphene prepared in our lab is 330 ± 20 Ω/sq, and decreases to 245 Ω/sq upon n-doping with the 2 nm dimer layer. The Hall-effect measurements were all performed in air. To avoid degradation by oxygen and moisture, the doped graphene films were encapsulated using solvent-free epoxy (LT-U001UV Adhesive, Lumtec), which was confirmed to have negligible influence on the electrical properties of graphene (Figure S1 in the Supporting Information). The type of doping is determined through the sign of the Hall voltage (Table 1), which confirms that the majority carriers switch from holes to electrons upon doping, in agreement with the negative shift of the DPs in the GFET measurements. Furthermore, the majority carrier density increases from 1.58×10^{13} cm^{-2} to 2.88

x 10^{13} cm^{-2} upon doping. The hole mobility in the as-loaded graphene is 1200 cm^2/Vs, consistent with values reported for CVD graphene.[45] The surface doping leads to a slightly smaller electron mobility to 890 cm^2/Vs. Mansour et al. reported a comparable reduction in Hall mobility when few ayer graphene is doped with $[RuCp^*Mes]_2$.[1] The transfer of electrons from the monomers increases the carrier density while leaving the ionized dopant ions on the surface of graphene. These ions act as charged impurities, which cause carrier scattering and reduce the Hall mobility.[1] Yet, despite the moderate decrease in carrier mobility, R_s is reduced overall due to the increase in carrier density.

Table 1. Sheet resistance, Hall voltage, majority carrier density and Hall mobility from van der Pauw and Hall measurements.

	as-loaded graphene	n-doped graphene
Sheet Resistance (Ω/**sq**)	330	245
Hall Voltage (V)	+1.42 x 10^{-2}	-0.78 x 10^{-2}
Carrier Density (cm^{-2})	1.58 x 10^{13}	2.88 x 10^{13}
Hall Mobility ($cm^2V^{-1}s^{-1}$)	1200	890

The DC excitation current is 1 mA, and the magnetic field is 3600 G.

The effectiveness of surface n-doped graphene as a cathode for electron injection in organic semiconductors is investigated next, via electron spectroscopy to determine interface energy-level alignment and current-voltage measurements to assess electron injection. The organic semiconductor used here is the electron-transport material (ETM) $POPy_2$. Secondary electron cutoff (SECO), valence-band spectra, and interface energy-level diagrams are shown in Figure 5a-7a for pristine and doped $POPy_2$ on as-loaded and doped graphene. In the first series of spectra ($POPy_2$ on as-loaded graphene), the initial graphene WF is 4.33 eV, close to the value of 4.45 eV reported in Figure 3a. The deposition of 0.5 nm $POPy_2$ decreases the WF by about 0.38 eV, an abrupt shift that is attributed to the formation of an interface dipole with its positive end pointing from the graphene towards the $POPy_2$ film, perhaps indicating that the P=O bonds are preferentially oriented towards the graphene. Incremental deposition of up to 10.5 nm of $POPy_2$ results in a further decrease of WF and a shift of the $POPy_2$ highest occupied molecular orbital (HOMO) towards higher binding energy. Over this thickness range (0.5 nm to 10.5 nm), both vacuum level (E_{vac}) and HOMO level shift by 0.45 eV and 0.39 eV, the latter indicating an upward molecular level bending (≥ 0.39 eV) in $POPy_2$ near the interface. Using the $POPy_2$ transport gap of 3.69 eV previously determined by UPS and inverse photoemission spectroscopy,[39] the full energy diagram of the interface can be constructed (Figure 5b). Given the measured HOMO position at 2.37 eV below E_F on the 10.5 nm film, the transport gap and the 0.39 eV band bending, the $POPy_2$ lowest unoccupied molecular orbital (LUMO) is estimated to be at ~1.71 eV above the graphene Fermi level, thus establishing the electron-injection barrier. This considerable barrier height is expected, since $POPy_2$ has a very low EA of 2.20 eV[39] and the as-loaded graphene has a WF of ~ 4.33 eV.

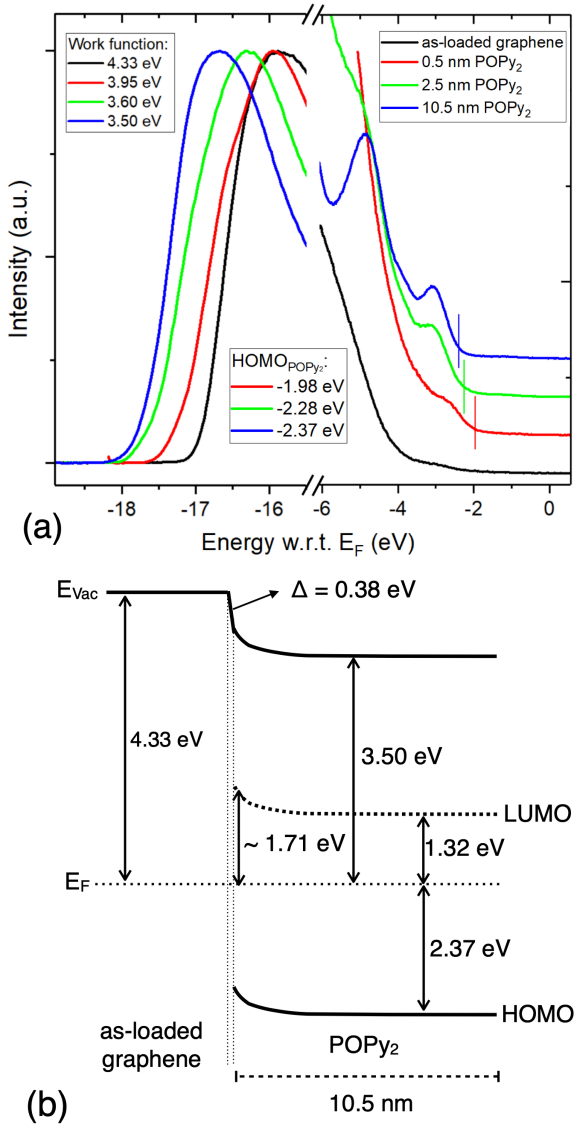

Figure 5. (a) Evolution of UPS photoemission onset and valence states as a function of $POPy_2$ deposited on as-loaded graphene. (b) Energy-level alignment at the interface between as-loaded graphene and $POPy_2$, as determined from UPS spectra.

Similar measurements conducted on $POPy_2$/doped graphene interfaces reveal a different evolution. In agreement with the data of Figure 2, the WF of graphene decreases from 4.35 eV to 2.61 eV with the deposition of 2 nm of $[RuCp^*Mes]_2$ followed by UV activation. Upon sequential deposition of pristine $POPy_2$, the WF slowly increases, reaching a final value of 3.03 eV for a 10 nm thick $POPy_2$ film, while the HOMO level shifts by about 0.34 eV toward lower binding energy (Figure 6a). The energy-level diagram of the interface is given in Figure 6b. The Fermi level at the surface of the organic film is now 0.83 eV below the LUMO, while the effective electron-injection barrier at the $POPy_2$/doped-graphene interface is reduced to 0.49 eV, a drastic reduction with respect to the previous case. Surface

doping of the graphene sheet appears therefore to be quite effective for changing the energy-level alignments at the interface. This will be confirmed below with electron-injection measurements.

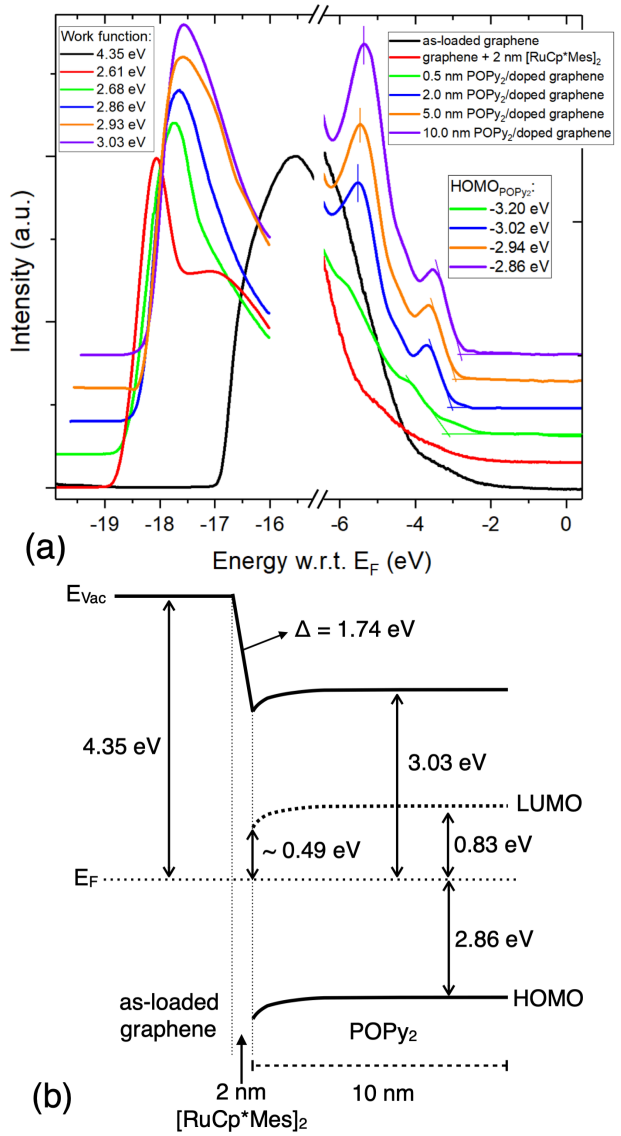

Figure 6. (a) Evolution of UPS photoemission onset and valence states as a function of $POPy_2$ deposited on graphene surface doped with 2 nm $[RuCp^*Mes]_2$. (b) Energy-level alignment at the interface between doped graphene and $POPy_2$, as determined from UPS spectra. The 1.74 eV reduction in graphene WF upon surface doping is the sum of two contributions, the surface dipole and the upward shift of the Fermi level.

Another frequently employed strategy to improve electron injection in OLEDs is to dope the ETL itself,[39,46] to reduce interface barriers, enhance bulk conductivity and fill deep traps in the band gap.[47,48] Therefore, in order to assess the differences between bulk and interfacial doping in the $POPy_2$/graphene system, we also investigated the energy level alignment between as-loaded graphene and n-doped $POPy_2$. The UPS spectra of graphene covered by incremental amounts of $POPy_2$ doped with $[RuCp^*Mes]_2$ (10 mol% + UV activation) are shown in Figure 7a. The doping ratio was chosen based on the optimal value reported in our previous work.[39] The as-loaded graphene exhibits a WF of 4.35 eV. The first deposition of n-doped $POPy_2$ (0.5 nm) reduces the WF to 2.98 eV by setting up an interface dipole, i.e. a partial electron transfer from the low work-function doped semiconductor to the graphene. This is followed by a more progressive reduction down to 2.54 eV for a film thickness of 10 nm, a value that is in excellent agreement with the WF determined by Xin et al. on similarly doped $POPy_2$.[39] The valence spectra also show new features between -3.0 and -0.5 eV below E_F, which are likely due to the reduced $POPy_2$ species stablized by proximity to $[RuCp^*Mes]^+$ cations. A linear estimation of the $POPy_2$ IE (HOMO onset) yields a 0.37 eV HOMO edge shift to higher binding energy as the film thickness increases from 0.5 nm to 10 nm. The Fermi level of the 10 nm doped $POPy_2$ film is 3.37 eV above the HOMO onset, which places it 0.32 eV below the LUMO onset. As deduced from the shift of the $POPy_2$ HOMO edge, there is an upward molecular-level bending of about 0.37 eV at the interface with graphene, and the effective electron-injection barrier is estimated to be about 0.69 eV (Figure 7b).

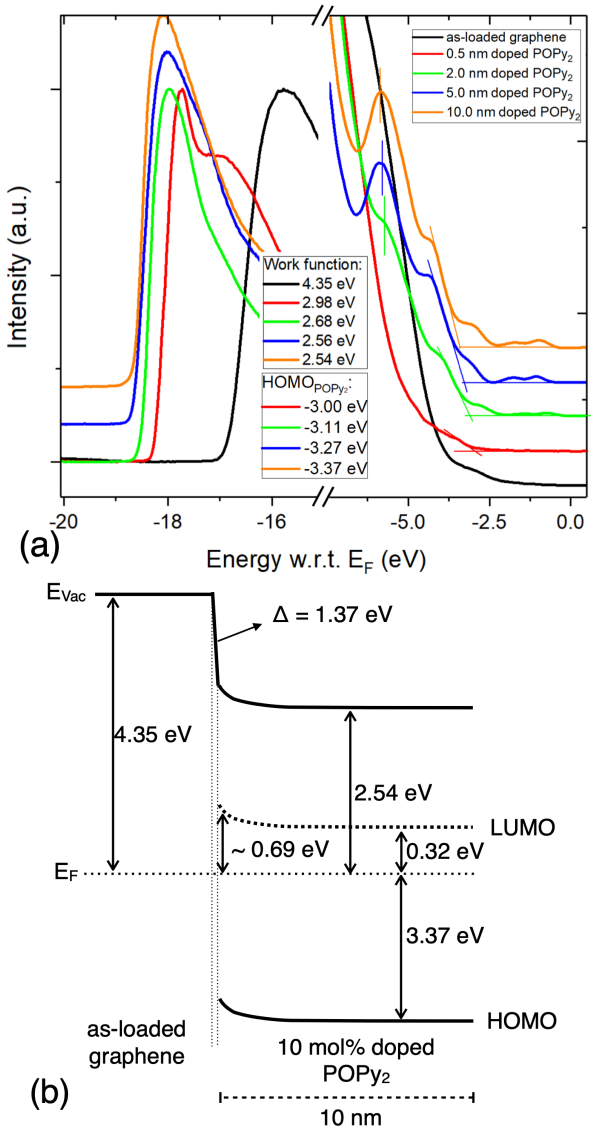

Figure 7. (a) Evolution of UPS photoemission onset and valence states as a function of 10 mol% bulk doped $POPy_2$ deposited on

as-loaded graphene. (b) Energy level alignment at the interface between as-loaded graphene and doped $POPy_2$, as determined from UPS spectra.

The UPS results indicate that surface doping significantly reduces the WF of graphene and changes the $POPy_2$/graphene interface energetics, resulting in an electron-injection barrier of 0.49 eV. Bulk doping in $POPy_2$, on the other hand, reduces the barrier height only to 0.69 eV, but increases the bulk conductivity of the $POPy_2$ layer.[39] To gain insight into the best option for electron injection enhancement compared to the undoped POPy2/as-loaded graphene system, we examine the current density - voltage (J-V) characteristics of three diodes: (1) as-loaded graphene/$POPy_2$/Al; (2) surface doped graphene:$[RuCp^*Mes]_2$ (2 nm)/$POPy_2$/Al, and (3) as-loaded grphene/$POPy_2$:$[RuCp^*Mes]_2$ (10 mol%)/Al. The thickness of the $POPy_2$ layer is chosen to be 200 nm to mitigate potential issues due to the nonuniformity of the film and leakage current in the diode. The three device structures and corresponding J-V characteristics are shown in Figure 8a,b. As expected, diode (1) shows nearly symmetric J-V characteristics, with a low current density of the order of 10^{-3} mA/cm^2 at +5 V. Poor electron injection from both Al and graphene is consistent with large injection barriers at both electrodes. In contrast, diode (2) exhibits asymmetric J-V characteristics, with significantly higher current density when the sample bias – positive bias on the top Al electrode – corresponds to electron injection from the surface-doped graphene (Figure 8a). The current at 4 or 5 V is more than three orders of magnitude larger in diode (2) than diode (1), consistent with the barrier lowering reported above. Diode (3) gives the largest electron current in both bias directions. Bulk doping in $POPy_2$ reduces injection barriers at both Al and as-loaded graphene interfaces, and also dramatically increases the $POPy_2$ conductivity, as reported by Xin et al.[39] The asymmetry in diode (3), in which the current injected in the diode from the top Al contact at V = -1 to -2 V is lower than that from the graphene under comparable positive bias, is presumably due to the reactive Al/$POPy_2$ interface.

Electron transport and n-doping in organic semiconductors exposed to air are usually degraded by electron trap states generated by oxygen and related complexes. These states are typically around 4 eV below vacuum level, below the electron-transport level (LUMO) of many organic semiconductors. Materials specifically designed for air-stable electron transport have an EA larger than ca. 4 eV, placing the electron-transport level at or below oxygen-related trap states. This is clearly not the case for $POPy_2$ (EA = 2.2 eV),

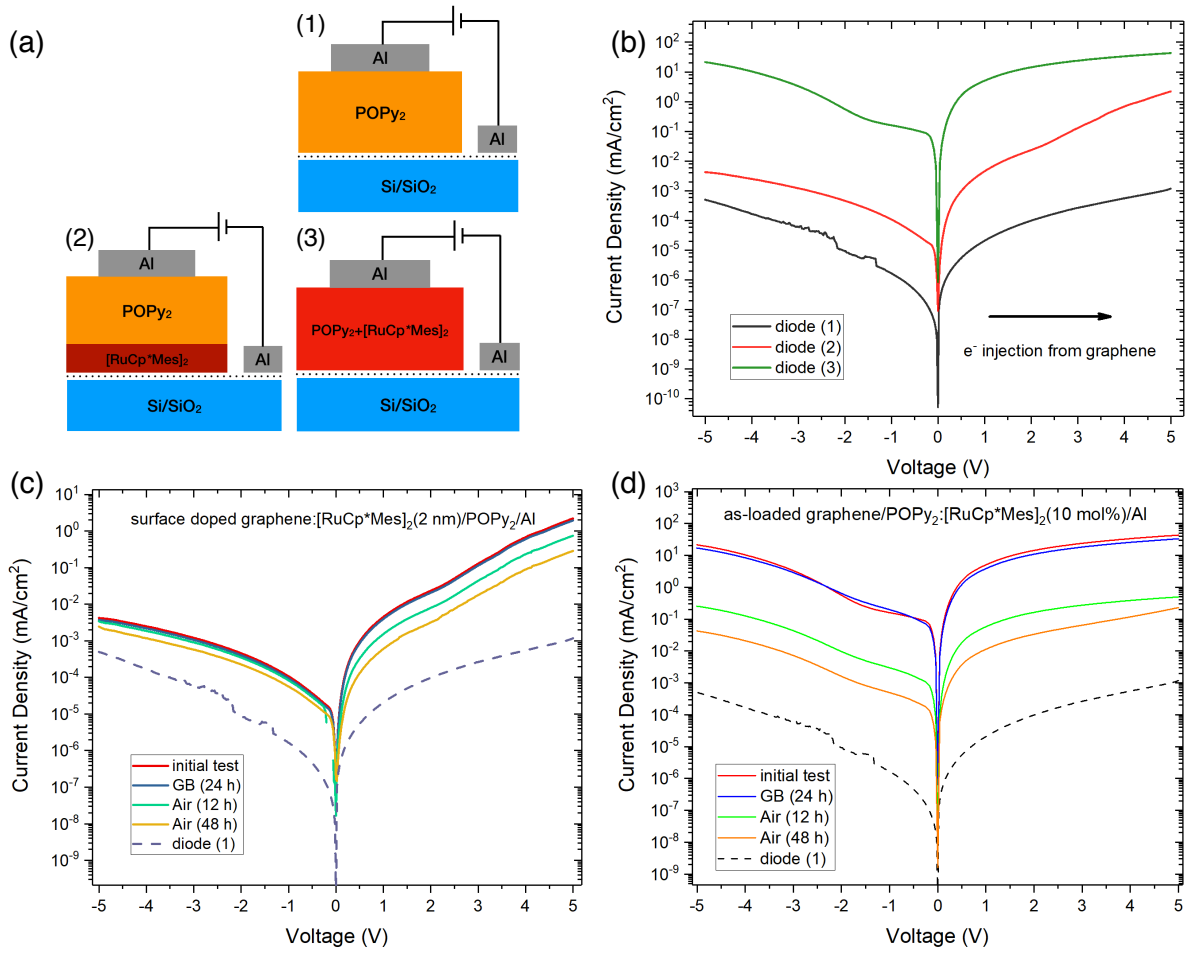

Figure 8. (a) schematics of three diode structures: (1) as-loaded graphene/$POPy_2$/Al, (2) surface doped graphene:$[RuCp^*Mes]_2$(2 nm)/$POPy_2$/Al, and (3) as-loaded graphene/$POPy_2$:$[RuCp^*Mes]_2$(10 mol%)/Al; (b) J-V characteristics of three diodes; (c)-(d) stability test on diode (2) and diode (3), measured after 24 h in glovebox (GB), 12 h in air, and 24 h in air. In each case the sign of the voltage corresponds to the polarity of the top Al electrode.

and n-doping of this material is, therefore, bound to be considerably reduced by exposure to ambient conditions. Here we investigate the relative air stability of diodes (2) and (3), in which the graphene electrode and of the $POPy_2$ layer, respectively, are doped. We measure the changes in J-V characteristics of the two devices placed in N_2 glovebox ($O_2 \leqslant$ 0.1 ppm) or ambient environment for up to 48 h. Exposure to N_2 in the glovebox for 24 h has negligible impact on the J-V characteristics of both diode (2) and diode (3), as can be seen from Figures 8c,d. Upon air exposure of diode (2) for 12 h and 48 h, however, the electron current injected from the surface-doped graphene (V>0, Figure 8c) is reduced by factors of 2.9 and 7.6, respectively. Yet, the current density after 48 h in air is still at least two orders-of-magnitude larger than in the undoped diode (1), showing moderate air stability. In contrast, diode (3) exhibits significantly less stability when exposed to air, with electron current densities injected from both contacts decreasing by two orders-of-magnitude after 12 h. This difference in air-stability likely originates with the different diode structures. In diode (2), the 200 nm $POPy_2$ layer covers the $[RuCp^*Mes]_2$ dopants deposited on the graphene surface and the resultant low-WF material, and works as a protective encapsulation layer. Even though oxygen penetration at the top of the organic layer contributes to some electron trapping, the $POPy_2$/doped graphene interface is mostly preserved. In diode (3), the doped $POPy_2$ layer is unprotected, oxygen and related complexes penetrate the layer, reduce the density of "free" electrons introduced by doping, and decrease the current density. Although both diode structures show degradation under air exposure, they stay reasonably stable in inert atmosphere (N_2). In practice, OLEDs will be encapsulated properly, and the results presented above suggest that devices with $[RuCp^*Mes]_2$ doped graphene cathode or bulk doped ETL should demonstrate reasonable performance stability in ambient environment.

■ CONCLUSION

In this work, we demonstrated the effective reduction of the electron-injection barrier between a single-layer graphene cathode and a very low-electron-affinity organic electron-transport material, $POPy_2$, via surface doping of the graphene layer. The graphene work function is reduced from 4.5 eV to a remarkably low value of 2.6 eV upon deposition of 1 nm of the molecular reductant $[RuCp^*Mes]_2$ and UV photoactivation, which enhances the electron-donation process. This reduction owes to the formation of a dipole between ionized dopants and graphene, as well as to the upward shift of the Fermi level above the Dirac point reflecting an increase in the free electron density of graphene. Photoemission spectroscopy, contact-potential measurements, and Hall-effect measurements confirm the dopant-induced changes in the electronic properties of the graphene layer. The effectiveness of electron injection from the low-work-function surface-doped graphene is demonstrated with a series graphene/$POPy_2$/Al diodes comprising either undoped graphene and $POPy_2$, surface-doped graphene, or bulk-doped $POPy_2$. The latter two devices show orders of magnitude increases in electron current. Finally, the device with surface doped graphene, which ensures more effective protection of the doped area, show reasonable ambient stability.

■ ASSOCIATED CONTENT

Supporting Information.
The Supporting Information is available free of charge on the ACS Publications website.

Experimental details and characterization data (PDF)

■ AUTHOR INFORMATION

Corresponding Author

* (A.K.) E-mail: kahn@princeton.edu

Notes

The authors declare no competing financial interest.

■ ACKNOWLEDGMENT

Work on molecular doping at Georgia Tech and Princeton was partly supported by the National Science Foundation (DMR-1305247, DMR-1506097 and DMR-1807797). Preparation of graphene at Ben-Gurion University of the Negev was supported by INNI – Israel National Nanotechnology Initiative under FTA programs.

■ REFERENCES

(1) Mansour, A. E.; Said, M. M.; Dey, S.; Hu, H.; Zhang, S.; Munir, R.; Zhang, Y.; Moudgil, K.; Barlow, S.; Marder, S. R.; Amassian, A. Facile Doping and Work-Function Modification of Few-Layer Graphene Using Molecular Oxidants axnd Reductants. Adv. Funct. Mater. 2017, 27, 1602004.

(2) Wu, C. C.; Wu, C. I.; Sturm, J. C.; Kahn, A. Surface Modification of Indium Tin Oxide by Plasma Treatment: An Effective Method to Improve the Efficiency, Brightness, and Reliability of Organic Light Emitting Devices. *Appl. Phys. Lett.* **1997**, *70*, 1348–1350.

(3)Ellmer, K. Development of Optically Transparent Electrodes. *Nat. Photonics.* **2012**, *6*, 809–817.

(4) Lee, S. T.; Gao, Z. Q.; Hung, L. S.; Lee, S. T.; Gao, Z. Q. Metal Diffusion from Electrodes in Organic Light-Emitting Diodes. *Appl. Phys. Lett.* **2005**, *75*, 1404–1406.

(5) Allen, M. J.; Tung, V. C.; Kaner, R. B. Honeycomb Carbon: A Review of Graphene. *Chem. Rev.* **2010**, *110*, 132-145.

(6) Han, T. H.; Lee, Y.; Choi, M. R.; Woo, S. H.; Bae, S. H.; Hong, B. H.; Ahn, J. H.; Lee, T. W. Extremely Efficient Flexible Organic Light-Emitting Diodes with Modified Graphene Anode. *Nat. Photonics.* **2012**, *6*, 105–110.

(7) Kim, J.; Hwang, J. H.; Suh, J.; Tongay, S.; Kwon, S.; Hwang, C. C.; Wu, J. Work Function Engineering of Single Layer Graphene by Irradiation-Induced Defects Work Function Engineering of Single Layer Graphene by Irradiation-Induced Defects. *Appl. Phys. Lett.* **2013**, *103*, 171604.

(8) Guo, B.; Fang, L.; Zhang, B.; Gong, J. R. Graphene Doping: A Review. *Insciences J.* **2011**, *1*, 80–89.

(9) Kim, K. S.; Bourlinos, A. B.; Otyepka, M.; Kim, N.; Hobza, P.; Zboril, R.; Georgakilas, V.; Kemp, K. C.; Chandra, V. Functionalization of Graphene: Covalent and Non-Covalent Approaches, Derivatives and Applications. *Chem. Rev.* **2012**, *112*, 6156–6214.

(10) Chen, Z.; Santoso, I.; Wang, R.; Xie, L. F.; Mao, H. Y.; Huang, H.; Wang, Y. Z.; Gao, X. Y.; Chen, Z. K.; Ma, D.; et al. Surface Transfer Hole Doping of Epitaxial Graphene Using MoO_3 thin Film. *Appl. Phys. Lett*. **2010**, *96*, 213104.

(11) Hellstrom, S. L.; Vosgueritchian, M.; Stoltenberg, R. M.; Irfan, I.; Hammock, M.; Wang, Y. B.; Jia, C.; Guo, X.; Gao, Y.; Bao, Z. Strong and Stable Doping of Carbon Nanotubes and Graphene by MoO_X for Transparent Electrodes. *Nano Lett.* **2012**, *12*, 3574–3580.

(12) Zurutuza, A.; Weatherup, R.; D'Arsié, L.; Centeno, A.; Cepek, C.; Robertson, J.; Bhardwaj, S.; Guo, Y.; Esconjauregui, S. Stability of Graphene Doping with MoO3 and I2. *Appl. Phys. Lett.* **2014**, *105*, 103103.

(13) Kwon, K. C.; Choi, K. S.; Kim, S. Y. Increased Work Function in Few-Layer Graphene Sheets via Metal Chloride Doping. *Adv. Funct. Mater.* **2012**, *22*, 4724–4731.

(14) Jeong, H. K.; Kim, K. J.; Kim, S. M.; Lee, Y. H. Modification of the Electronic Structures of Graphene by Viologen. *Chem. Phys. Lett.* **2010**, *498*, 168–171.

(15)Sun, T.; Wang, Z.; Shi, Z.; Ran, G.; Xu, W.; Wang, Z.; Li, Y.; D ai, L.; Qin, G. Multilayered Graphene Used as Anode of Organic Light Emitting Devices. *Appl. Phys. Lett.* **2010**, *96*, 133301.

(16) Chen, J.; Jang, C.; Adam, S.; Fuhrer, M. S.; Williams, E. D.; Ishigami, M. Charged-Impurity Scattering in Graphene. *Nat. Phys.* **2008**, 4, 377–381.

(17) Wei, D.; Liu, Y.; Wang, Y.; Zhang, H.; Huang, L.; Yu, G. Synthesis of N-Doped Graphene by Chemical Vapor Deposition and Its Electrical Properties. *Nano Lett.* **2009**, *9*, 1752–1758.

(18) Wang, Y.; Shao, Y.; Matson, D. W.; Li, J.; Lin, Y. Nitrogen-Doped Graphene and Its Application in Electrochemical Biosensing. *ACS Nano* **2010**, *4*, 1790–1798.

(19) Cai, Y.; Wei, H. X.; Li, J.; Bao, Q. Y.; Zhao, X.; Lee, S. T.; Li, Y. Q.; Tang, J. X. Mechanism of Cs_2CO_3 as an N-Type Dopant in Organic Electron-Transport Film. *Appl. Phys. Lett.* **2011**, *98*, 113304.

(20) Kwon, K. C.; Choi, K. S.; Kim, B. J.; Lee, J. L.; Kim, S. Y. Work-Function Decrease of Graphene Sheet Using Alkali Metal Carbonates. *J. Phys. Chem. C* **2012**, *116*, 26586–26591.

(21) Pi, K.; McCreary, K. M.; Bao, W.; Han, W.; Chiang, Y. F.; Li, Y.; Tsai, S. W.; Lau, C. N.; Kawakami, R. K. Electronic Doping and Scattering by Transition Metals on Graphene. *Phys. Rev. B.* **2009**, *80*, 075406.

(22) Giovannetti, G.; Khomyakov, P. A.; Brocks, G.; Karpan, V. M.; Van Den Brink, J.; Kelly, P. J. Doping Graphene with Metal Contacts. *Phys. Rev. Lett.* **2008**, *101*, 026803.

(23) Hill, E. W.; Novoselov, K. S.; Geim, A. K.; Katsnelson, M. I.; Blake, P.; Morozov, S. V.; Schedin, F. Detection of Individual Gas Molecules Adsorbed on Graphene. *Nat. Mater.* **2007**, 6, 652–655.

(24) Li, X.; Wang, H.; Robinson, J. T.; Sanchez, H.; Diankov, G. Simultaneous Nitrogen Doping and Reduction of Graphene Oxide. *J. Am. Chem. Soc.* **2009**, *13*, 15939–15944.

(25) Wang, X.; Li, X.; Zhang, L.; Yoon, Y.; Weber, P. K.; Wang, H.; Guo, J.; Dai, H. N-Doping of Graphene Through Electrothermal Reactions with Ammonia. *Science* **2009**, *324*, 768–771.

(26) Kasry, A.; Kuroda, M. A.; Martyna, G. J.; Tulevski, G. S.; Bol, A. A. Electrodes, C. Chemical Doping of Large-Area Stacked Graphene Films for Use as Transparent, Conducting Electrodes. *ACS Nano* **2010**, *4*, 3839–3844.

(27) Wehling, T. O.; Novoselov, K. S.; Morozov, S. V.; Vdovin, E. E.; Katsnelson, M. I.; Geim, A. K.; Lichtenstein, A. I. Molecular Doping of Graphene. *Nano Lett.* **2008**, *8*, 173–177.

(28) Paniagua, S. A.; Baltazar, J.; Sojoudi, H.; Mohapatra, S. K.; Zhang, S.; Henderson, C. L.; Graham, S.; Barlow, S.; Marder, S. R. Production of Heavily N- and p-Doped CVD Graphene with Solution-Processed Redox-Active Metal-Organic Species. *Mater. Horizons* **2014**, *1*, 111–115.

(29) Watcharinyanon, S.; Virojanadara, C.; Johansson, L. I. Rb and Cs Deposition on Epitaxial Graphene Grown on 6H -SiC (0001). *Surf. Sci.* **2011**, *605*, 1918–1922.

(30) Guo, B.; Liu, Q.; Chen, E.; Zhu, H.; Fang, L.; Gong, J. R. Controllable N-Doping of Graphene. *Nano Lett.* **2010**, *10*, 4975–4980.

(31) Faccio, R.; Ferna, L.; Pardo, H.; Goyenola, C. Electronic and Structural Distortions in Graphene Induced by Carbon Vacancies and Boron Doping. *J. Phys. Chem. C* **2010**, *114*, 18961–18971.

(32) Pinto, H.; Markevich, A. Electronic and Electrochemical Doping of Graphene by Surface Adsorbates. *Beilstein J. Nanotechnol.* **2014**, *5*, 1842–1848.

(33) Wei, P.; Liu, N.; Lee, H. R.; Adijanto, E.; Ci, L.; Naab, B. D.; Zhong, J. Q.; Park, J.; Chen, W.; Cui, Y.; Bao, Z. Tuning the Dirac Point in CVD-Grown Graphene through Solution Processed N-Type Doping with 2-(2-Methoxyphenyl)-1,3-Dimethyl- 2,3-Dihydro-1H-benzoimidazole. *Nano Lett.* **2013**, *13*, 1890–1897.

(34) Derivatives, H.; Naab, B. D.; Guo, S.; Olthof, S.; Evans, E. G. B.; Wei, P.; Millhauser, G. L.; Kahn, A.; Barlow, S.; Marder, S. R.; Bao, Z.. Mechanistic Study on the Solution-Phase N-Doping of 1,3-Dimethyl- 2-Aryl-2,3-Dihydro-1H-benzoimidazole Derivatives. *J. Am. Chem. Soc.* **2013**, *135*, 15018–1502.

(35) Akaike, K.; Nardi, M. V; Oehzelt, M.; Frisch, J.; Opitz, A.; Christodoulou, C.; Ligorio, G.; Beyer, P.; Timpel, M.; Pis, I.; et al. Effective Work Function Reduction of Practical Electrodes Using an Organometallic Dimer. *Adv. Funct. Mater.* **2016**, *26*, 2493–2502.

(36) Giordano, A. J.; Pulvirenti, F.; Khan, T. M.; Fuentes-hernandez, C.; Moudgil, K.; Delcamp, J. H.; Kippelen, B.; Barlow, S.; Marder, S. R. Organometallic Dimers : Application to Work-Function Reduction of Conducting Oxides. *ACS Appl. Mater. Interf.* **2015**, *7*, 4320–4326.

(37) Guo, S.; Kim, S. B.; Mohapatra, S. K.; Qi, Y.; Sajoto, T.; Kahn, A.; Marder, S. R.; Barlow, S. N-Doping of Organic Electronic Materials Using Air-Stable Organometallics. *Adv. Mater.* **2012**, *24*, 699–703.

(38) Mohapatra, S. K.; Fonari, A.; Risko, C.; Yesudas, K.; Moudgil, K.; Delcamp, J. H.; Timofeeva, T. V.; Brédas, J. L.; Marder, S. R.; Barlow, S. Dimers of Nineteen-Electron Sandwich Compounds: Crystal and Electronic Structures, and Comparison of Reducing Strengths. *Chem. - A Eur. J.* **2014**, *20*, 15385–15394.

(39) Lin, X.; Wegner, B.; Lee, K. M.; Fusella, M. A.; Zhang, F.; Moudgil, K.; Rand, B. P.; Barlow, S.; Marder, S. R.; Koch, N.; Kahn, A. Beating the Thermodynamic Limit with Photo-Activation of n-Doping in Organic Semiconductors. *Nat. Mater.* **2017**, *16*, 1209–1215.

(40) Ryu, S.; Liu, L.; Berciaud, S.; Yu, Y. J.; Liu, H.; Kim, P.; Flynn, G. W.; Brus, L. E. Atmospheric Oxygen Binding and Hole Doping in Deformed Graphene on a SiO_2 Substrate. *Nano Lett.* **2010**, *10*, 4944–4951.

(41) Guo, S.; Mohapatra, S. K.; Romanov, A.; Timofeeva, T. V.; Hardcastle, K. I.; Yesudas, K.; Risko, C.; Brédas, J. L.; Marder, S. R.; Barlow, S. N-Doping of Organic Electronic Materials Using Air-Stable Organometallics: A Mechanistic Study of Reduction by Dimeric Sandwich Compounds. *Chem. - A Eur. J.* **2012**, *18*, 14760–14772.

(42) Zhang, S.; Naab, B. D.; Jucov, E. V.; Parkin, S.; Evans, E. G. B.; Millhauser, G. L.; Timofeeva, T. V.; Risko, C.; Brédas, J. L.; Bao, Z.; et al. N-Dopants Based on Dimers of Benzimidazoline Radicals: Structures and Mechanism of Redox Reactions. *Chem. - A Eur. J.* **2015**, *21*, 10878–10885.

(43) Pirkle, A.; Chan, J.; Venugopal, A.; Hinojos, D.; Magnuson, C. W.; McDonnell, S.; Colombo, L.; Vogel, E. M.; Ruoff, R. S.; Wallace, R. M. The Effect of Chemical Residues on the Physical and Electrical Properties of Chemical Vapor Deposited Graphene Transferred to SiO_2. *Appl. Phys. Lett.* **2011**, *99*, 122108.

(44) Xu, W.; Lim, T. S.; Seo, H. K.; Min, S. Y.; Cho, H.; Park, M. H.; Kim, Y. H.; Lee, T. W. N-Doped Graphene Field-Effect Transistors with Enhanced Electron Mobility and Air-Stability. *Small* **2014**, *10*, 1999–2005.

(45) Song, H. S.; Li, S. L.; Miyazaki, H.; Sato, S.; Hayashi, K.; Yamada, A.; Yokoyama, N.; Tsukagoshi, K. Origin of the Relatively Low Transport Mobility of Graphene Grown through Chemical Vapor Deposition. *Sci. Rep.* **2012**, *2*, 337.

(46) Pfeiffer, M.; Leo, K.; Zhou, X.; Huang, J. S.; Hofmann, M.; Werner, A.; Blochwitz-Nimoth, J. Doped Organic Semiconductors: Physics and Application in Light Emitting Diodes. *Org. Electron.* **2003**, *4*, 89–103.

(47) Olthof, S.; Singh, S.; Mohapatra, S. K.; Barlow, S.; Marder, S. R.; Kippelen, B.; Kahn, A. Passivation of Trap States in Unpurified and Purified C_{60} and the Influence on Organic Field-Effect Transistor Performance. *Appl. Phys. Lett.* **2012**, *101*, 253303.

(48) Olthof, S.; Mehraeen, S.; Mohapatra, S. K.; Barlow, S.; Coropceanu, V.; Brédas, J. L.; Marder, S. R.; Kahn, A. Ultralow Doping in Organic Semiconductors: Evidence of Trap Filling. *Phys. Rev. Lett.* **2012**, *109*, 1176601.

TOC